# Uptake on fractal particles 1. Theoretical framework

Daniel Coelho, Slimane Bekki, Jean-François Thovert, Pierre Marie Adler

JOURNAL OF GEOPHYSICAL RESEARCH, VOL. 105, NO. D3, PAGES 3905-3916, FEBRUARY 16, 2000

# Uptake on fractal particles 1. Theoretical framework

Daniel Coelho,[1] Slimane Bekki,[2] Jean-Francois Thovert,[3] and Pierre M. Adler[1]

**Abstract.** We develop a detailed framework for calculating uptake rates of gases on fractal particles. Aggregates with a fractal dimension between 1.6 and 2.6 are generated numerically. Three-dimensional simulations of uptake on these aggregates are performed for a large range of conditions. The numerical results can be expressed by a single physically based formula as a function of the usual parameters (gas phase diffusion coefficient, uptake coefficient) and of morphological parameters (aggregate gyration radius, size of the monomers composing the aggregate, fractal dimension). The expression for the uptake flux on an aggregate is generalized to a lognormal distribution of aggregates. The results for an isolated aggregate are compared to calculations used for spherical particles. The importance of accounting for the fractal character of aggregates in the calculation of the uptake flux is highlighted. The magnitude of the errors also depends on which aggregate equivalent size is used as the characteristic radius for mass transfer.

## 1. Introduction

Carbonaceous aerosols produced by combustion processes, also called smoke or soot, often consist of aggregates which are composed of numerous elementary particles or monomers. These aggregates exhibit a self-similar structure which implies a fractal morphology in that the number of monomers and the radius of gyration of the aggregate are linked by a power law relationship [*Forrest and Witten*, 1979; *Mandelbrot*, 1982; *Schmidt-Ott*, 1988; *Meakin*, 1991]. Carbonaceous aerosols are found throughout the lower atmosphere with biomass burning and fossil fuel combustion being the main sources in the troposphere [*Penner et al.*, 1993; *Cooke and Wilson*, 1996]. They have long been recognized as a major local pollutant in urban areas. They are also considered as a significant contributor to climate forcing because they strongly absorb solar radiation and may act as cloud condensation nuclei [*Haywood and Shine*, 1995; Intergovernmental Panel on Climate Change, 1996; *Schult et al.*, 1997]. Finally, by interacting with gaseous chemical species, they may play a significant role in atmospheric chemistry [*Pueschel et al.*, 1992; *Blake and Kato*, 1995].

Uptake processes on carbonaceous aerosols have been increasingly studied recently. Atmospheric measurements indicate that water uptake on aircraft-generated carbonaceous aerosols might contribute to contrail and cloud formation [*Karcher et al.*, 1996; *Minnis et al.*, 1998; *Strom and Ohlsson*, 1998]. Cloud nucleating properties and water uptake on carbonaceous material are also actively investigated in laboratory [*Lammel and Novakov*, 1995; *Chughtai et al.*, 1996; *Weingartner et al.*, 1997]. In addition, chemical observations combined with modeling studies suggest that uptake, reactive or not, of certain gases on carbonaceous aerosols could influence the nitrogen and ozone budget in the troposphere and lower stratosphere [*Smyth et al.*, 1996; *Jacob et al.*, 1996; *Hauglustaine et al.*, 1996; *Lary et al.*, 1997; *Bekki*, 1997; *Aumont et al.*, 1999; *Lary et al.*, 1999]. Several laboratory experiments have already been devoted to the determination of the uptake coefficients [*Tabor et al.*, 1994; *Fendel et al.*, 1995; *Smith and Chughtai*, 1996; *Rogaski et al.*, 1997; *Kalberer et al.*, 1996; *Ammann et al.*, 1998]. Interestingly, uptake of chemical species such as ozone alters the physicochemical properties of the carbonaceous surfaces and, consequently, influences the water uptake properties [*Vartiainen et al.*, 1996; *Kotzick et al.*, 1997]. This underlines the link between heterogeneous chemical reactivity and cloud nucleating properties of carbonaceous aerosols.

Most of these laboratory and modeling studies would probably benefit from a rigorous framework for calculating mass transfers and uptake rates on fractal mate-

[1]Institut de Physique du Globe de Paris, Paris.
[2]Service d'Aéronomie du Centre National de la Recherche Scientifique, Université P. et M. Curie, Paris.
[3]Laboratoire des Phénomènes de Transport dans les Mélanges, Futuroscope, France.



Paper number 1999JD900815.
0148-0227/00/1999JD900815$09.00

rial (S.G. Jennings et al., Carbonaceous aerosol fractal surface area: Implications for heterogeneous chemistry, submitted to *Geophysical Research Letters*, 1999). The uptake rate depends on a number of parameters such as the reaction probability, also called accommodation coefficient in the case of a nonreactive uptake, the size or surface area of the particle and a correction factor. This correction factor allows the continuum regime diffusion equation to be used for the transition and free molecular regime; it accounts for the competition between diffusion of the chemical species in the gas phase and accommodation or reaction at the surface. The surface area and the correction factor are usually calculated using some size characterization specific to an instrument technique. Comparing these various sizes is not trivial because they may describe radically different particle dynamics. The uptake is often assumed to be reaction limited, giving a simple proportional dependency of the rate on the surface area. Methods for calculating the surface area can differ considerably. In some studies, the surface area is assumed to be equal to the sum of the surfaces of the monomers composing the aggregates. In other studies the fractal structure of the particles or material is completely neglected. For example, the surface area of a carbonaceous sample in laboratory experiments is often taken as the geometric surface area of the macroscopic sample.

The purpose of this work is to provide a framework for calculating rates of uptake, reactive or not, on fractal aggregates and to assess how much information on the aggregate morphology is required in order to perform accurate calculations. The paper is organized as follows. The second section is devoted to some background on the numerical generation of fractal aggregates and on the resolution of the diffusion/reaction equation. A large range of fractal particles is considered in this study. They have morphologies similar to observed carbonaceous aerosols. The third section describes the numerical three-dimensional simulations of uptake on isolated aggregates. The main results are discussed. Simple physically based relationships are derived from the numerical results in section 4. The important parameters regarding the particle structure are highlighted. Finally, in section 5 the new relationships are compared to the expressions of the spherical particles. The importance of taking into account the fractal character of aggregates in this type of calculations is highlighted.

## 2. Modeling

### 2.1. Aggregate Generation

An aggregate or cluster can be characterized by its gyration radius $R_G$ which may be defined as

$$R_G^2 = \frac{1}{2N^2} \sum_{n,m=1}^{N} (\mathbf{r}_n - \mathbf{r}_m)^2 , \qquad (1)$$

where $N$ is the total number of particles of the aggregate; $n$ and $m$ denote the number of any two monomers and $\mathbf{r}_n$ is the position vector of particles. For the sake of numerical simplicity in the present study, each monomer is supposed to be a cube of size $a$.

The fractal dimension $D_F$ may be introduced by the relation

$$N = \zeta \left(\frac{R_G}{a}\right)^{D_F} , \qquad (2)$$

where $\zeta$ is the compacity of the aggregate.

Many procedures have been proposed in the literature [*Jullien and Botet*, 1987] for generating aggregates with various fractal dimensions. Three of them have been selected here to study the dependence of the results on the mode of construction of the aggregates [*Coelho et al.*, 1997]. Since theses models have been described in detail previously, we only recall briefly the different ways the fractal aggregates are constructed and the relevant characteristics of the aggregates. Note that our model-generated aggregates are very similar to carbonaceous aerosols observed in the atmosphere [*Bekki et al.*, this issue].

A modified Witten and Sander scheme was used in order to accelerate the convergence to the asymptotic regime [*Witten and Sander*, 1981]. The random particle does not stick to the aggregate when it is on a site adjacent to occupied sites, but it is moved until it is on an occupied site; then its final position is supposed to be the previous one. Such a scheme yields a fractal dimension of 2.64, which is slightly larger than the value of 2.5 obtained with the original Witten and Sander scheme.

The hierarchical model with linear trajectories was applied without any modifications [*Sutherland*, 1970]; two aggregates of same size $N$ are assumed to stick when they occupy adjacent sites. Their resulting fractal dimension is difficult to measure with precision because of the large statistical fluctuations due to the model itself; it was found to be close to 1.9.

The last model is a hierarchical model where the fractal dimension is tuned by selecting the orientation and the sticking point of aggregates of size $2^{(p-1)}$ where $p$ is the iteration number [*Thouy and Jullien*, 1994]. Four values of the fractal dimension were studied, namely, 1.6, 1.9, 2.2, and 2.5. For comparison purposes, two of them were chosen close to the values of the Witten-Sander aggregate and to the standard hierarchical model.

The structures of some of the aggregates are represented in Figure 1. Each aggregate is placed inside a large cubic cell of size $N_c.a$ and its properties computed. $N_c$ was chosen equal to 32, 48, 64, and 96. In order to minimize the influence of the finite size of the cell, the center of gravity of each aggregate is assumed to be located at the center of this cubic cell. Usually, $N_c.a$ is taken large enough with respect to the gyration radius so that the resulting fraction of the large cubic cell volume occupied by solid particles is smaller than 0.02.

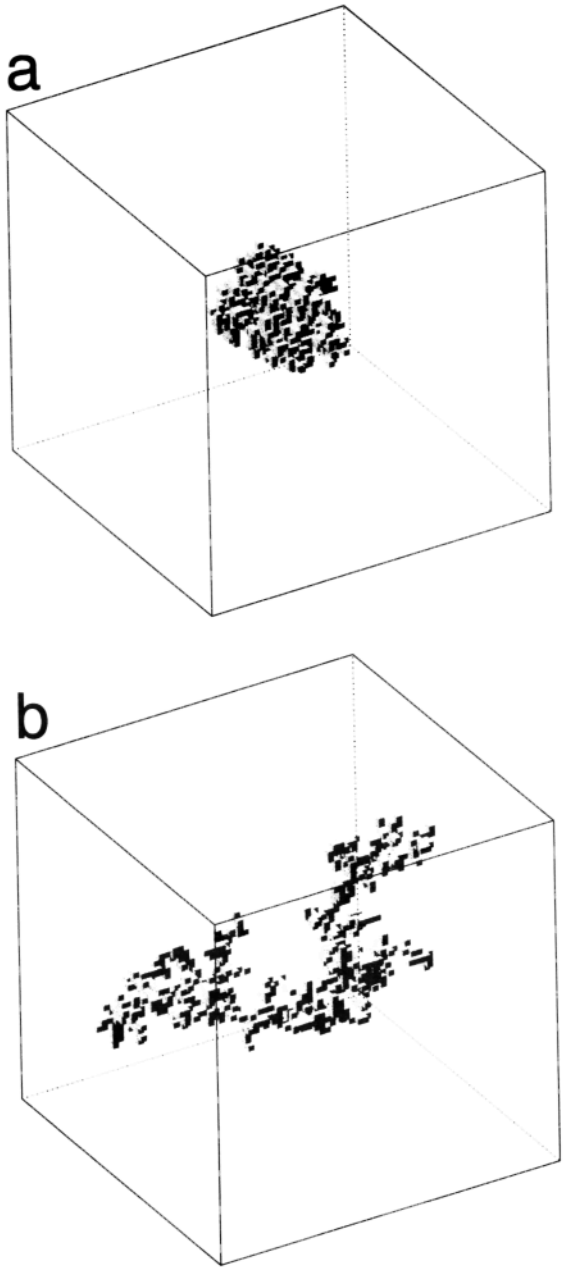


**Figure 1.** Examples of fractal aggregates composed of cubic particles of size a; they are located inside cubic boxes of size 64*a*. (a) The aggregate was built with a modified Witten and Sander scheme. (b) The aggregate was built with the hierarchical model.

The morphological parameters relative to these aggregates are summarized in Table 1. The values of fractal dimension considered here cover approximately the range of values observed in atmospheric carbonaceous aerosols (see Table 2 of the companion paper [*Bekki et al.*, this issue]). Values of the compacity $\zeta$ can be compared to previous studies of soot aggregates composed of spherical monomers. In this case, the relationship equivalent to (2) is

$$N = k_0 \left(\frac{R_G}{r}\right)^{D_F}, \quad (3)$$

where $k_0$ is called the prefactor or structural coefficient and is equivalent to $\zeta$; $r$ is the radius of the spherical monomers. If the spherical monomers of such aggregates are replaced by cubic monomers of size equal to the diameter of the spherical monomers, the radius of gyration remains unchanged. Therefore combining (2) and (3) gives $k_0 \sim \zeta/2^{D_F}$.

A number of three-dimensional numerical simulations [*Sorensen and Roberts*, 1997; *Oh and Sorensen*, 1997] and laboratory experiments [*Cai et al.*, 1995; *Sorensen and Feke*, 1996] have been performed on soot with a fractal dimension of about 1.8. They found that $k_0$ ranges between 1.2 and 1.3 for most cases. The prefactor $k_0$ calculated from $\zeta$ and $D_F$ given in Table 1 varies from 1 to 1.3 for aggregates with $D_F$ close to 1.8 ($D_F$=1.9 and 1.6), which is consistent with the previous results.

### 2.2. Mass Transfer and Boundary Conditions

For numerical reasons, aggregates must be represented within a limited three-dimensional domain, the external cell. Consider a chemical species whose concentration is $C$, which diffuses from the walls $\partial\varsigma$ of the cell to the surface of the aggregate where it undergoes a pseudo-first-order loss or chemical conversion. If a constant concentration $C_\infty$ is maintained on $\partial\varsigma$, a permanent concentration field is obtained in the cell. The situation, where the size of the cell is very large compared to the size of the aggregate, is the most relevant to atmospheric problems, where aggregates are immersed in an infinite fluid, the air, with uniform concentration far from the aggregates.

The steady state mass transfer to the aggregate is ruled in the bulk by the classical diffusion equation

$$\nabla.(D\nabla C) = 0, \quad (4)$$

where $D$ is the gas phase diffusion coefficient of the species.

Boundary conditions are as follows. At the surface of the cell,

$$C = C_\infty. \quad (5)$$

At the surface $S_{\text{fractal}}$ of the aggregate with the unit external normal $\mathbf{n}$

$$\mathbf{n}.D\nabla C = K_s\, C \text{ on } S_{\text{fractal}}, \quad (6)$$

where $K_s$ is the surface reaction rate constant, which may be called the uptake velocity. It is related to the reaction probability $\gamma$ (or sticking probability in the case of a nonreactive uptake), which is defined as the ratio of the number of reactive collisions to the total number of collisions, by the following relationship

$$K_s = \frac{\gamma.v}{4},$$

where v is the molecular velocity of the species.

**Table 1.** The Fractal Dimension $D_F$ and the Compacity $\zeta$ of the Various Types of Aggregates

| | Witten/Sander | Hierarchical | Thouy/Jullien | | | |
|---|---|---|---|---|---|---|
| | $D_F$=2.64 | $D_F$=1.90 | $D_F$=1.6 | $D_F$=1.9 | $D_F$=2.2 | $D_F$=2.5 |
| $N$=64 | 4.13±0.22 | 3.80±0.07 | 3.83 | 4.23 | 4.03 | 4.40 |
| $N$=256 | 4.34±0.14 | 3.71±0.12 | 3.82 | 4.19 | 3.96 | 4.26 |
| $N$=1024 | 4.48±0.13 | 3.66±0.26 | 3.82 | 4.18 | 3.94 | 4.20 |

In this steady state regime, one is mostly interested by the mass flux $J$ of a diffusing species which reacts at the surface of the aggregate. $J$ is given by

$$J = \oint D\, d\mathbf{S}.\nabla C\,, \tag{7}$$

where $\mathbf{S}$ is any closed surface which surrounds the aggregate.

### 2.3. Analytical Results for Spheres

We start by recalling the case of compact spheres because analytical results are available and should help to interpret the numerical results on fractal aggregates. Let us consider two concentric spheres of radii $R_i$ and $R_e$. Equations (5) and (6) hold on the external and the internal spheres, respectively. Because of the spherical symmetry, the concentration field is easily calculated as well as the flux $J$,

$$J = 4\pi D C_\infty R_i \left(\frac{R_i}{\tilde{R}} + \frac{1}{\mathrm{PeDa}}\right)^{-1}, \tag{8}$$

where

$$\frac{1}{\tilde{R}} = \frac{1}{R_i} - \frac{1}{R_e}\,, \tag{9}$$

$$\mathrm{PeDa} = \frac{K_s R_i}{D}\,, \tag{10}$$

where PeDa, called the Peclet-Dahmköhler number, is the correction factor mentioned in the introduction. It is a dimensionless quantity which compares the surface chemical rate to the gas phase diffusion rate. It is somewhat similar to the diffuso-reactive parameter which is used in the calculation of loss rates in liquid spheres when the chemical reaction takes place within the liquid [*Hanson et al.*, 1994]; the diffuso-reactive parameter compares the chemical rate to the liquid diffusion rate. For clarity we will call the Peclet-Dahmköhler number the reaction/diffusion ratio.

The most relevant case here is an isolated particle of radius $R$ (immersed in an infinite fluid, so $R_e \to \infty$). Hence $\tilde{R} = R_i = R$ and the flux can be written as

$$J_{\mathrm{sphere}} = 4\pi D C_\infty R \left(1 + \frac{1}{\mathrm{PeDa}}\right)^{-1}. \tag{11}$$

It is convenient to introduce a dimensionless quantity, the Nusselt number $Nu$, which is defined as the ratio of the actual flux $J$ to the diffusion flux, which would be the actual flux if the uptake was diffusion limited.

$$Nu = \frac{J}{4\pi D C_\infty R}\,, \tag{12}$$

leading to

$$Nu = \left(1 + \frac{1}{\mathrm{PeDa}}\right)^{-1}. \tag{13}$$

We will call $Nu$ the scaled flux. When PeDa$\gg$1, $Nu = 1$. The uptake is said to be diffusion limited and the flux is given by

$$J_{\mathrm{sphere}} = 4\pi D C_\infty R\,.$$

When PeDa$\ll$1, $Nu$ = PeDa. The uptake is reaction limited and the flux becomes proportional to the surface area,

$$J_{\mathrm{sphere}} = 4\pi K_s C_\infty R^2\,,$$

Between these two established regimes lies the transition regime where the uptake is controlled by both processes and the full relationship (11) has to be used.

Equations (10) and (11) can be found under other equivalent forms in the literature [*Turco et al.*, 1989; *Ghosh et al.*, 1995; *Seinfeld and Pandis*, 1998]. For example, the flux can also be expressed as a function of $\gamma$ and the Knudsen number $Kn$ which compares the mean free path $l_a$ of the diffusing species in the fluid, here air, and the size of the sphere,

$$Kn = \frac{l_a}{R}\,. \tag{14}$$

When $Kn\ll$1 (i.e., the mean free path of the diffusing species is much smaller than the size of the sphere), the sphere is said to be in the continuum regime. In the limit of $Kn\gg$1, the sphere is said to be in the free molecular or kinetic regime.

Since $l_a$=3$D/v$ [*Turco et al.*, 1989; *Seinfeld and Pandis*, 1998], PeDa can be expressed as a function of $Kn$,

$$\mathrm{PeDa} = \frac{3\gamma}{4\,Kn}\,. \tag{15}$$

Mass transfer in the diffusion limited regime implies necessarily a continuum regime. We prefer to use PeDa instead of $Kn$ for characterizing the nature of the uptake because, unlike $Kn$, PeDa also accounts for the number of collisions leading to the uptake of the species. In the following sections, non-spherical aggregates in a cubic cell are considered and the diffusion equation is solved numerically.

## 3. Numerical Results

Equation (4) and the related boundary conditions (5) and (6) were discretised in three dimensions (see Figure 1) by the finite volume technique and solved by an improved version of conjugate gradient; this represents an extension and a significant progress on the first versions of this technique [*Thovert et al.*, 1990].

The geometry of the problem is characterised by several parameters which can be listed as follows: the size $N_c.a$ of the cell, the number $N$ of monomers of the aggregate (or equivalently its gyration radius $R_G$), and some statistical characteristics of the geometry of the aggregate such as its fractal dimension $D_F$.

The size $N_c.a$ of the cell is not a physically meaningful parameter for our purposes; it is only of interest here in the limit $N_c.a \to \infty$. Similarly, the number $N$ of monomers of the aggregate should be large enough so that it is in the limiting fractal regime (i.e., $D_F$ independent of $N$ or size of the aggregate).

In order to study these parameters, two sets of numerical simulations were performed over wide intervals of variations. Six kinds of random aggregates with fractal dimensions ranging from 1.6 to 2.64 were considered (see Table 1). In the first series of simulations, $N_c$ and $N$ were set equal to

$N_c$=32, 48, 64, 96
$N$=64, 256, 1024

Also, eight different values of the reaction coefficient $K_s$ were used, corresponding to a dimensionless coefficient $K_s$.a/D equal to $10^n$ with $n$=-4,-3,-2,-1,-0.5,0,0.5,1. For each case, 10 aggregates were generated and the resulting concentration fields solved numerically.

In addition to the first series, a second series of simulations was designed to study the diffusion limited regime specifically. The boundary condition (5) was replaced by a Dirichlet condition at the surface of the aggregate: $C = 0$ on $S_{\text{fractal}}$ (i.e., $K_s.a/D \to \infty$).

A larger set of values for $N_c$ and $N$ was used in the second series,

$N_c$=32, 48, 64, 80, 96
$N$= 32, 64, 128, 256, 512, 1024

By analogy with spherical aggregates, the scaled flux $Nu$ and the reaction/diffusion ratio PeDa are initially based on the gyration radius,

$$(\text{PeDa})_G = \frac{K_s R_G}{D}$$

$$(Nu)_G = \frac{J}{4\pi D C_\infty R_G} .$$

In order to limit the range of values on the flux axis, results for the first series of simulations are represented under the form of $(Nu)_G$ as a function of $(\text{PeDa})_G$ in Figure 2. The solid line corresponds to the scaled flux calculated from (11). Numerical results are the symbols. This representation shows a lot of scatter, suggesting that $Nu$ and PeDa defined from the radius of gyration cannot fully account for the results. This scat-

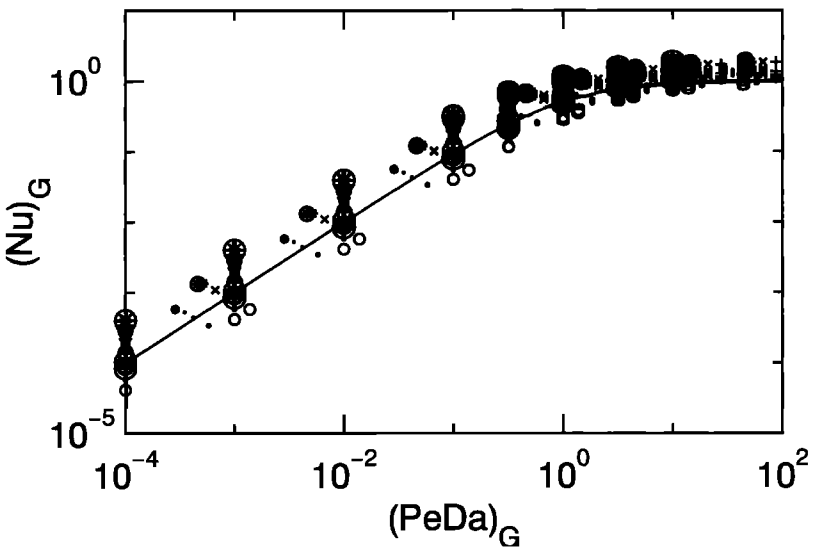


**Figure 2.** Scaled flux $(Nu)_G$ as a function of the reaction/diffusion ratio $(\text{PeDa})_G$ for the first series of simulations. The solid line corresponds to $Nu$ calculated from the uptake flux given by (11). Each point represents an average over 10 simulations. Data symbols are crosses in circles for the modified Witten and Sander model ($D_F$=2.64), pluses in circles for the hierachical model with linear trajectories ($D_F$=1.9), circles for the Thouy and Jullien model ($D_F$=1.6), pluses for the Thouy and Jullien model ($D_F$=1.9), crosses for the Thouy and Jullien model ($D_F$=2.2) and asterisks for the Thouy and Jullien model ($D_F$=2.5).

ter originates from the fact that, unlike spheres, a length scale is not sufficient for characterizing the morphology of fractal aggregates. More parameters are required.

## 4. Derivation of Physically Based Relationships

The general strategy for simplifying this complex picture is to study the dependence of the numerical results on these parameters and derive physically based fits which are consistent with the analytical results of the sphere, the final aim being to cast the results into a form similar to (11) with adequate definitions of the various quantities. This will be done by considering the two asymptotic regimes, large and small values of PeDa.

In the diffusion limited regime (PeDa$\gg$1), a characteristic length of the aggregate, henceforth referred to as diffusion equivalent radius $R_d$, is defined in such a way that

$$J = 4\pi D C_\infty R_d . \tag{16}$$

In the reaction limited regime (PeDa$\ll$1),

$$J = K_s S_{\text{fractal}} C_\infty , \tag{17}$$

where $S_{\text{fractal}}$ is the surface area of the aggregate. Hence PeDa can be expressed as

$$\text{PeDa} = \frac{K_s S_{\text{fractal}}}{4\pi D R_d} . \tag{18}$$

By fitting the upper and lower limits, it is hoped that the whole set of numerical results will lie on the curve calculated using (18). The following section is devoted to the determination of $R_d$ and $S_{\text{fractal}}$.

### 4.1. Determination of the Diffusion Equivalent Radius

Let us first analyze the influence of the artificial parameter $N_c.a$ which is the size of the external cell. By analogy with (9), $1/R_d$ derived from the numerical results is plotted as a function of $1/(N_c.a)$ in Figure 3. Each straight line corresponds to a specific aggregate inside cells of various sizes. Within few percents, the slopes are identical and equal to 2, which demonstrates that $R_e$ and $N_c.a/2$ are equivalent. An expression similar to (9) can then be derived,

$$\frac{1}{R_d} = \frac{1}{R_{d\infty}} - \frac{2}{N_c.a} , \tag{19}$$

where $R_{d\infty}$ is the diffusion equivalent radius of an aggregate in an infinite fluid.

The next step consists of analysing the relationship which exists between the diffusion equivalent radius and the gyration radius. On physical grounds, $R_{d\infty}$ is expected to be proportional to $R_G$. $R_{d\infty}$ is displayed as a function of $R_G$ in Figure 4. Each straight line corresponds to aggregates built according to the same rule, but with different $R_G$. Hence the linear relationship which is supported by the numerical results is given by

$$R_{d\infty} = \alpha(D_F).R_G + \beta(D_F) . \tag{20}$$

In the following, $\beta(D_F)$ can be neglected for sufficiently large aggregates.

The last step consists of analysing $\alpha$ as a function of $D_F$. This is done in Figure 5, where the scale tends to magnify the variations. A linear regression fit yields

$$\alpha(D_F) = 0.4755.D_F - 0.0537 , \tag{21}$$

with a regression coefficient of 0.96. Since $D_F$ is greater

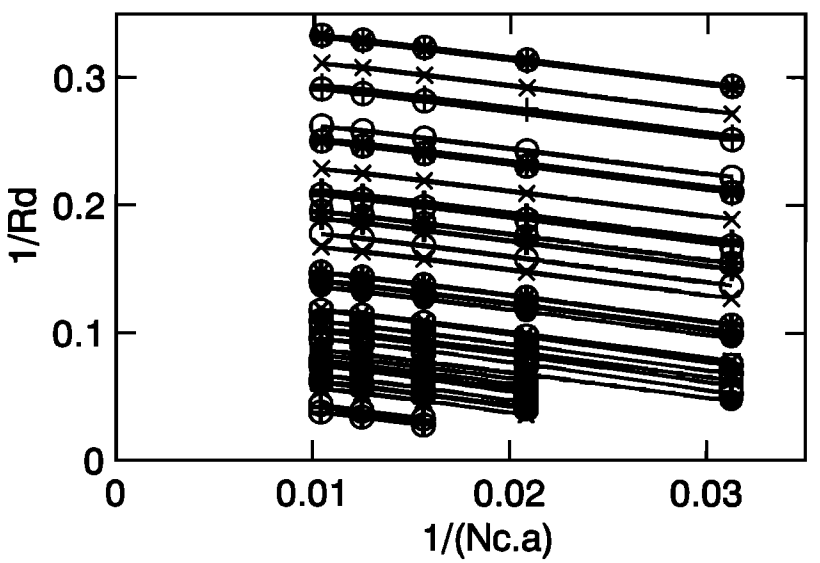


**Figure 3.** Inverse diffusion radius $1/R_d$ as a function of $1/(N_c.a)$ for the second series of simulations (PeDa $\to \infty$). Each straight line corresponds to a given aggregate ($D_F$ and $N$ constant) inside cells of different sizes. Each point represents an average over 10 simulations. Data symbols are the same as in Figure 2; data for spheres are represented by solid circles.

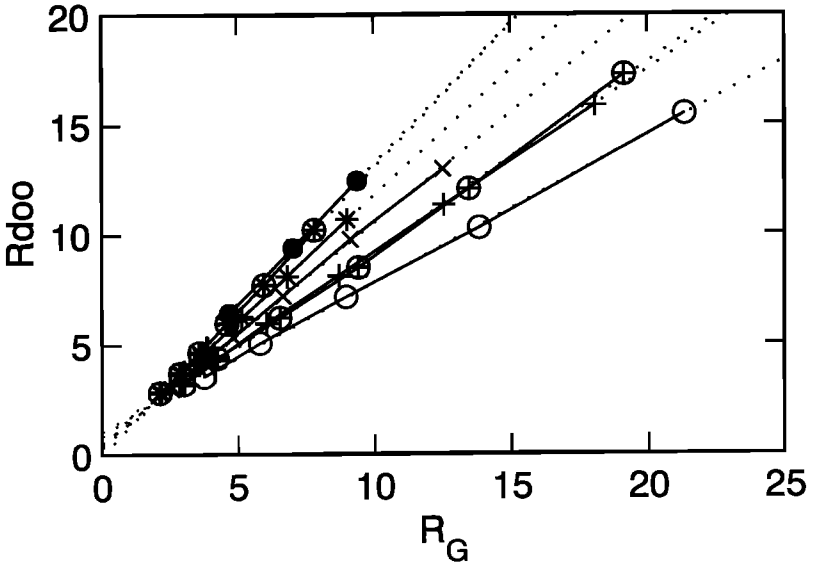


**Figure 4.** Diffusion equivalent radius $R_{d\infty}$ as a function of the gyration radius $R_G$. Each line corresponds to the same type of aggregates. Data symbols are the same as in Figure 3.

than unity, a simple proportionality relationship reproduces reasonably well the numerical results,

$$\alpha(D_F) = 0.45\, D_F \,. \tag{22}$$

Combining (19), (20) and (21), the diffusion equivalent radius of fractal aggregate in an external cell of size $N_c.a$ can be expressed as

$$\frac{1}{R_d} = \frac{1}{0.45\, D_F\, R_G} - \frac{2}{N_c.a} \,. \tag{23}$$

If the aggregate is isolated (i.e., in infinite fluid), $R_d$ is given by

$$R_{d\infty} = 0.45\, D_F\, R_G \,. \tag{24}$$

### 4.2. Determination of the Aggregate Surface Area

In order to determine the value of PeDa as expressed in (18), the surface of the aggregate needs to be calculated. $S_{\text{fractal}}$ may be defined as the surface in contact with the fluid, here the air; for instance, when two cubic monomers of size $a$ are in contact with one another, the total surface of this two-cubes aggregate is $10.a^2$. On intuitive grounds, $S_{\text{fractal}}$ may have been expected to scale as $R_G^{D_F-1}$, but this is not verified by our numerical simulations. In fact, $S_{\text{fractal}}$ should be expressed with respect to the number $N$ of monomers composing

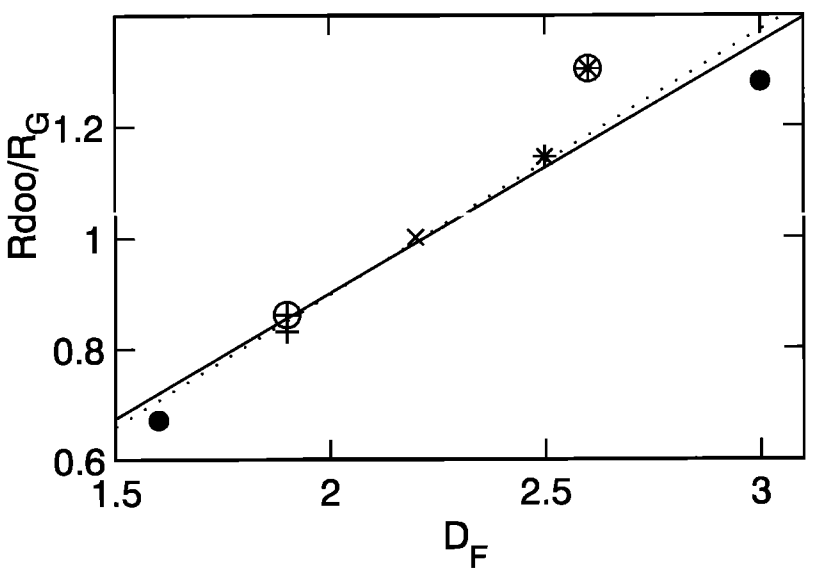


**Figure 5.** $R_{d\infty}/R_G$ as a function of the fractal dimension $D_F$. The dotted line corresponds to the linear regression fit (22) and the solid line to the proportionality relationship (23). Data symbols are the same as in Figure 3.

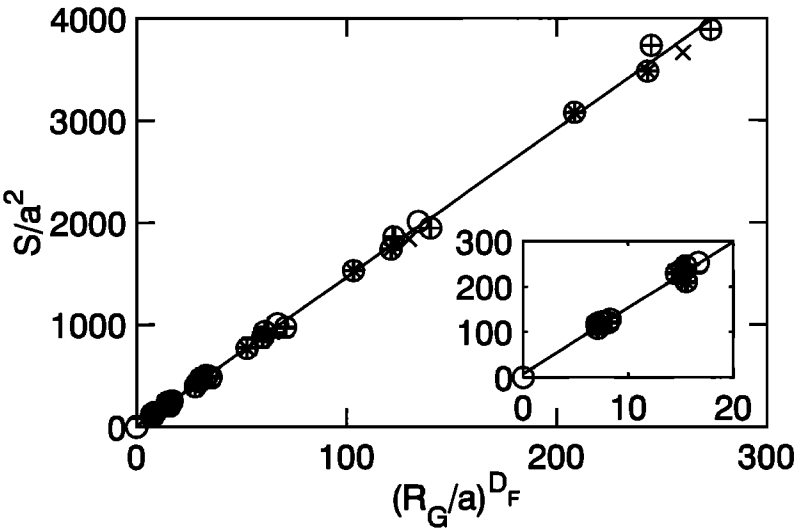


**Figure 6.** Scaled surface area $S_{\text{fractal}}/a^2$ as a function of $(R_G/a)^{D_F}$. The subplot is an enlarged view for small aggregates. The solid line corresponds to the linear regression fit (27). Data symbols are the same as in Figure 3.

the aggregate,

$$S_{\text{fractal}} = s\,N \tag{25}$$

with

$$s = F\,s_o\,,$$

where $s_o$, $s$ and $F$ are the surface of an isolated monomer ($= 6\,a^2$), the averaged free surface area of the monomers (surface in contact with the fluid, which is air here), and the averaged fraction of free surface on the monomers, respectively.

By substituting $N$, (25) becomes

$$S_{\text{fractal}} = F\,6\,a^2\,\zeta\left(\frac{R_G}{a}\right)^{D_F}. \tag{26}$$

All the numerical data are plotted as functions of $R_G^{D_F}$ in Figure 6. A linear regression yields

$$\frac{S_{\text{fractal}}}{a^2} = 14.4\left(\frac{R_G}{a}\right)^{D_F} , +10 \tag{27}$$

with a correlation coefficient of 0.9991. For large aggregates the constant 10 can be omitted.

It is somewhat remarkable that the proportionality coefficient between $S_{\text{fractal}}$ and $R_G^{D_F}$ is the same for all the type of aggregate considered here. The mode of construction of the aggregates does not appear to have any influence. This indicates that the averaged fraction of free surface area $F$ of the monomers is inversely proportional to the compacity $\zeta$ of the aggregate. In our calculations, $\zeta$ varies from 3.6 to 4.5, which is equivalent to $F_w$ varying from 53% (on average, 3.2 faces out of the 6 faces of the cubic monomers are in contact with the fluid) to 67% (4 faces). In view of the rather limited number of aggregate types considered in this study, we cannot claim that the proportionality between $S_{\text{fractal}}$ and $R_G^{D_F}$ is valid for all fractal aggregates. In addition, only a limited range of $D_F$ has been tested.

### 4.3. Uptake Flux on an Isolated Fractal Aggregate

For practical purposes it might be useful to go back to dimensional quantities. We limit ourselves to the case of an isolated aggregate within an infinite fluid. Since the diffusion equivalent radius $R_{d\infty}$ and $S_{\text{fractal}}$ are given by (24) and (27), respectively, the flux $J_{\text{fractal}}$ may be expressed as

$$J_{\text{fractal}} = 5.65\,D\,C_\infty\,D_F\,R_G\left(1 + \frac{1}{\text{PeDa}}\right)^{-1} \tag{28}$$

where

$$\text{PeDa} = \frac{K_s\,R_G}{D}\,\frac{2.55}{D_F}\left(\frac{R_G}{a}\right)^{(D_F-2)}. \tag{29}$$

The fact that $J_{\text{fractal}}$ scales as $R_G$ in the diffusion limited regime and as $R_G^{D_F}$ in the reaction limited regime is generally consistent with previous calculations [*Meakin et al.*, 1989; *Schmidt-Ott et al.*, 1990]. However, in the reaction limited regime (which corresponds to the free molecular/kinetic regime for a high reaction probability $\gamma$), we did not find that $J_{\text{fractal}}$ scales as $R_G^2$ for $D_F > 2$ [*Schmidt-Ott et al.*, 1990]. It might be possible that one needs to consider aggregates composed of an extremely large number of monomers in order to detect this dependency [*Meakin et al.*, 1989].

Equation (28) can be tested for the extreme case of compact spheres (i.e., $R_G = \sqrt{3/5}R$, $a = R$ and $D_F = 3$). In the diffusion limited regime, $J_{\text{fractal}}$ is equal to $J_{\text{sphere}}$ within 5%. However, in the reaction limited regime (when J is proportional to the surface area), $J_{\text{fractal}}$ and $J_{\text{sphere}}$ differ by almost a factor 2. This may correspond

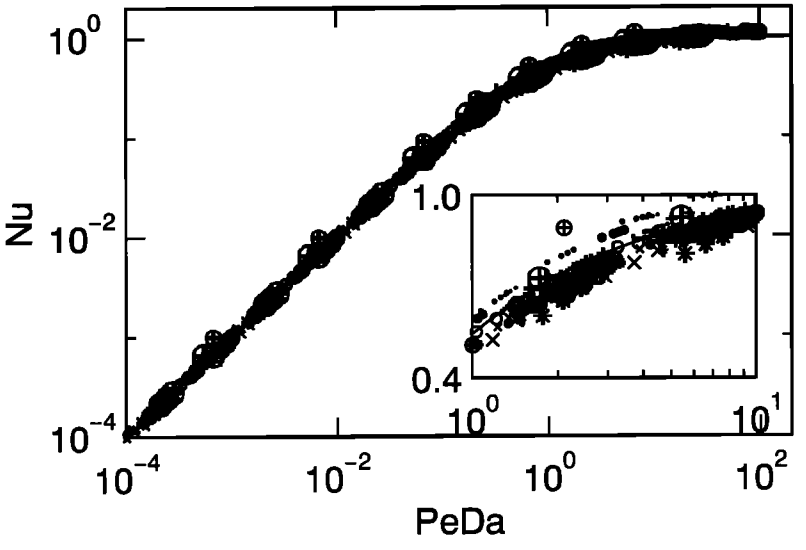


**Figure 7.** Scaled flux $Nu$ as a function of the reaction/diffusion ratio PeDa. The solid line corresponds to $Nu$ calculated from the uptake flux given by (28). Each point represents an average over 10 simulations. The subplot is an enlarged view of the transition regime. Data symbols are the same as in Figure 3.

to the distinction between the free surface area $S_e$ which is in contact with the external fluid (fluid connected to infinity) and the surface area $S_i$ which bounds closed fluid cavities within the aggregate. As long as $D_F$ is not too close to 3, $S_{\text{fractal}} \sim S_e$. However, when aggregates are highly compact with $D_F$ approaching 3, some closed fluid cavities may form and $S_i$ becomes significant. This type of extreme case is not often encountered in the atmosphere and therefore no further numerical study was devoted to this topic. Overall, when $D_F$ tends towards 3, it is preferable to use the relationship (11).

In order to test (28) for more common cases of fractal aggregates, the scaled flux Nu can be plotted as a function of the reaction/diffusion ratio PeDa, as in Figure 2. For clarity, Nu is recalled to be

$$Nu = \frac{J}{5.65\, D\, C_\infty\, D_F\, R_G} . \tag{30}$$

All the numerical results (symbols) are displayed in Figure 7 where they are compared to the theoretical relationship (28). The agreement between the numerical results and (28) is found to be excellent; an enlarged view of the transition regime is given in the subplot of Figure 7. The improvement on relationship (11) is most obvious when comparing Figures 2 and 7. This demonstrates that the new framework performs in a satisfactory manner.

### 4.4. Extension to a Lognormal Distribution of Aggregates

Equation (28) corresponds to isolated single size fractal aggregates and hence can only be applied directly to monodispersed size distributions of aggregates. Before being applied to realistic cases, it needs to be generalized to aggregate populations with wider size distribution.

The total flux $J_t$ of a chemical species onto a distribution of fractal aggregates is given by

$$J_t = \int_0^\infty J_{\text{fractal}}\, N(R_G)\, dR_G , \tag{31}$$

where $N(R_G)$ is the size distribution.

Since many soot distributions tend to be lognormal [*Pueschel*, 1996; *Pueschel et al.*, 1998; *Reid and Hobbs*, 1998; *Reid et al.*, 1998], $N(R_G)$ is taken as

$$N(R_G)\, dR_G = \frac{N_0}{2\pi} \exp(-\frac{\alpha^2}{2})\, d\alpha \tag{32}$$

with

$$\alpha = \frac{\ln(R_G) - \ln(R_{G,\text{mod}})}{\ln(\sigma)} ,$$

where $N_0$, $R_{G,\text{mod}}$, and $\sigma$ are the total concentration, the mode radius, and the geometric standard deviation (also called the width) of the distribution of soot aggregates.

Equation (31) can be integrated analytically in the two asymptotic regimes using

$$\int_0^\infty R_G^A\, N(R_G)\, dR_G = \frac{R_{G,\text{mod}}^A\, N_0}{2\pi} \cdot \int_{-\infty}^{\infty} \exp(A \ln(\sigma)\, \alpha - \frac{\alpha^2}{2})\, d\alpha .$$

In the diffusion limited regime (PeDa$\gg$1), the uptake flux becomes

$$J_{t-\text{diff.}} = 5.65 D C_\infty D_F R_{G,\text{mod}} N_0 \exp\left(\frac{\ln^2(\sigma)}{2}\right) . \tag{33}$$

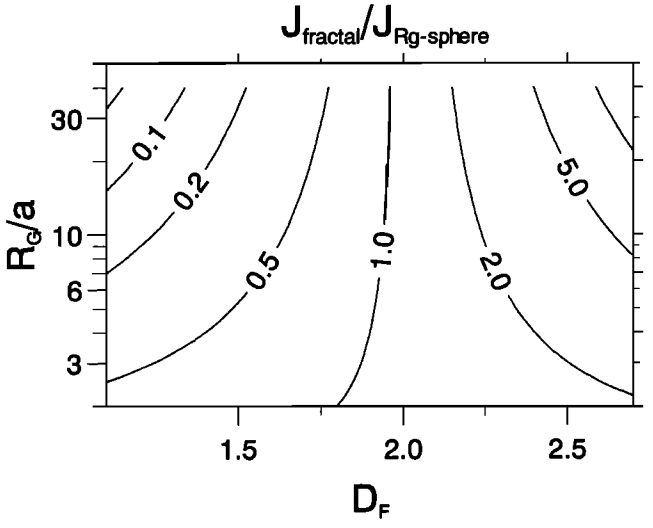


**Figure 8.** Ratio of the uptake fluxes $J_{\text{fractal}}/J_{Rg-\text{sphere}}$ as a function of the fractal dimension $D_F$ and $(R_G/a)$.

In the reaction limited regime (PeDa$\ll$1),

$$J_{t-\text{reac.}} = 14.4\, K_s\, C_\infty\, a^{(2-D_F)}\, R_{G,\text{mod}}^{D_F}\, N_0 \cdot \exp\left(\frac{(2-D_F^2)\,\ln^2(\sigma)}{2}\right). \quad (34)$$

If the size distribution is not too wide, the uptake flux in the transition regime can be approximated by

$$J_{t(\text{approx.})} = 5.65\, D\, C_\infty\, D_F \int_0^\infty R_G\, N(R_G)\, dR_G \cdot \left(1 + \frac{D\, D_F\, a^{(D_F-2)}}{2.55\, K_s} \cdot \frac{\int_0^\infty R_G\, N(R_G)\, dR_G}{\int_0^\infty R_G^{D_F}\, N(R_G)\, dR_G}\right)^{-1}. \quad (35)$$

After integration,

$$J_{t(\text{approx.})} = 5.65\, D\, C_\infty\, D_F\, R_{G,\text{mod}}\, N_0 \cdot \exp\left(\frac{\ln^2(\sigma)}{2}\right)\left(1 + \frac{1}{\text{PeDa}}\right)^{-1} \quad (36)$$

with

$$\text{PeDa} = \frac{K_s\, R_{G,\text{mod}}}{D}\,\frac{2.55}{D_F} \cdot \left(\frac{R_{G,\text{mod}}}{a}\right)^{(D_F-2)} \exp\left(\frac{(1-D_F^2)\,\ln^2(\sigma)}{2}\right).$$

As expected, this expression of PeDa is equal to $J_{t-\text{reac.}}/J_{t-\text{diff.}}$.

Once the flux is determined, the time constant $\tau$ for the uptake of a chemical species on a population of fractal aggregate can be derived from [*Ghosh et al.*, 1995]

$$\tau = \frac{C_\infty}{J_{\text{fractal}}}.$$

The uptake rate for the pseudo-first-order process is simply the reciprocal of $\tau$.

## 5. Fractal Versus Spherical Geometry

Some previous calculations of mass transfer to aggregates have been based on the assumption that the aggregates are compact spheres. In order to illustrate the errors generated when the fractal character of the aggregate is neglected, the uptake flux on a fractal aggregate $J_{\text{fractal}}$ is compared to the flux on a sphere. In order to estimate the magnitude of the errors, the sphere radius is arbitrarily taken to be equal to the gyration radius $R_G$. We call the flux of a sphere, defined with the gyration radius, $J_{Rg-\text{sphere}}$. In the diffusion limited regime, combining (11) and (28) yields to the ratio of the fluxes

$$J_{\text{fractal}}/J_{Rg-\text{sphere}} = 0.45\, D_F. \quad (37)$$

In this regime, $J_{\text{fractal}}$ is independent of the small-scale features such as the size of the monomers. The aggregate acts as a sphere of a radius equal to the gyration radius multiplied by about half of the fractal dimension.

In the reaction limited regime, uptake fluxes are directly proportional to the surface area. The ratio of the fluxes is given by

$$J_{\text{fractal}}/J_{Rg-\text{sphere}} = 1.15\left(\frac{R_G}{a}\right)^{(D_F-2)}. \quad (38)$$

It is displayed as a function of $R_G/a$ and $D_F$ in Figure 8. For a fractal dimension close to 2, aggregates can be treated as spheres with a radius equal approximatively to the gyration radius. However, when $D_F$ deviates significantly from 2, $J_{\text{fractal}}$ and $J_{Rg-\text{sphere}}$ can differ substantially (up to an order of magnitude for large elongated branch-like aggregates). It must be emphasized that the expressions (37) and (38) result from the use of the aggregate gyration radius as a sphere radius in (11). Other choices of equivalent size such as the aggregate volume mean radius or hydrodynamic radius would lead to different flux ratios and hence to different errors which could be substantially larger. The question of which aggregate equivalent size provides the best estimate of the mass transfer equivalent radius is tackled in the companion paper [*Bekki et al.*, this issue]. The variations seen in Figure 8 reflect the dependency of the surface area on $R_G/a$ and $D_F$. According to (26), increasing $R_G/a$ at fixed gyration radius (i.e., reducing the size of the monomers) has two opposite effects on $S_{\text{fractal}}$: it increases the number $N$ of monomers composing the aggregate, but it also decreases the surface area of the monomers. The overall effect is controlled by the aggregate structure, which is characterized by the fractal dimension.

In conclusion, the results reported here suggest that neglecting the fractal character in the calculation of uptake rates on aggregates may lead to flawed results, especially in the reaction limited regime for large aggregates (aggregates composed of numerous monomers).

Comparisons with three-dimensional numerical simulations show that relatively accurate calculations can be performed using the simple relationships presented in this paper. A full morphological characterization of the fractal aerosols is required in some cases.

**Acknowledgments.** The support of the French Programme National de la Chimie Atmosphérique (PNCA) is gratefully acknowledged.

## References

Ammann, M., M. Kalberer, D.T. Jost, L. Tobler, E. Rossler, D. Piguet, H.W. Gaggeler, and U. Baltensperger, Heterogeneous production of nitrous acid on soot in polluted air masses, *Nature, 395*, 157-160 , 1998.

Aumont, B., S. Madronich, M. Ammann, M. Kalberer, U. Baltensperger, D. Hauglustaine, and F. Brocheton, On the NO2 plus soot reaction in the atmosphere *J. Geophys. Res., 104*, 1729-1736, 1999.

Bekki, S., On the possible role of aircraft generated soot in middle latitude ozone depletion, *J. Geophys. Res., 102*, 10751-10758, 1997.

Bekki, S., C. David, K. Law, D.M. Smith, D. Coelho, J.-F. Thovert, and P.M. Adler, Uptake on fractal particles, 2, Applications, *J. Geophys. Res.*, this issue.

Blake, D.F., and K. Kato, Latitudinal distribution of black carbon soot in the upper troposphere and lower stratosphere, *J. Geophys. Res., 100*, 7195-7202, 1995.

Cai, J., N. Lu, and C.M. Sorensen, Analysis of fractal cluster morphology parameters - Structural coefficient and density autocorrelation function cutoff, *J. Colloid Interface Sci., 171*, 470-473, 1995.

Chughtai, A.R., M.E. Brooks, and D.M. Smith, Hydration of black carbon, *J. Geophys. Res., 101*, 19,505-19,514, 1996.

Coelho, D., J.-F. Thovert, R. Thouy, and P.M. Adler, Hydrodynamic drag and electrophoresis of suspensions of fractal aggregates, *Fractals, 5*, 507-522, 1997.

Cooke W.F., and J.N. Wilson, A global black carbon aerosol model, *J. Geophys. Res., 101*, 19,395-19,409, 1996.

Fendel, W., D. Matter, H. Burtscher, and A. Schmidt-Ott, Interaction between carbon or iron aerosol-particles and ozone, *Atmos. Environ., 29*, 967-973, 1995.

Forrest, S.R., and T.A. Witten, Long-range correlations in smoke-particule aggregates, *J. Phys. A Math Gen., 12*, 109-117, 1979.

Ghosh, S., D.J. Lary, and J.A. Pyle, Estimation of heterogeneous reaction rates for stratospheric trace gases with particular reference to the diffusional uptake of HCl and $ClONO_2$ by polar stratospheric clouds, *Ann. Geophys., 13*, 406-412, 1995.

Hanson, R.H., A.R. Ravishankara, and S. Solomon, Heterogeneous reactions in sulfuric acid aerosols: A framework for model calculations, *J. Geophys. Res., 99*, 3615-3629, 1994.

Hauglustaine, D.A., B.A. Ridley, S. Solomon, P.G. Hess, and S. Madronich, $HNO_3/NO_x$ ratio in the remote troposphere during MLOPEX 2: Evidence for nitric acid reduction on carbonaceous aerosols?, *Geophys. Res. Lett., 23*, 2609-2612, 1996.

Haywood, J.M., and K.P. Shine, The effect of anthropogenic sulfate and soot aerosol on the clear-sky planetary radiation budget, *Geophys. Res. Lett., 22*, 603-606, 1995.

Intergovernmental Panel on climate Change, *Climate Change 1995: The Science of Climate Change*, edited by J.T. Houghton et al., Cambridge Univ. Press, New York, 1996.

Jacob, D.J., et al., Origin of ozone and $NO_x$ in the tropical troposphere: A photochemical analysis of aircraft observations over the South Atlantic basin, *J. Geophys. Res., 101*, 24,235-24,250, 1996.

Jullien R., and R. Botet, *Aggregation and Fractal Aggregates*, World Sci., River Edge, N. J., 1987.

Kalberer, M., et al., Heterogeneous chemical processing of $(NO_2)$-N-13 by monodisperse carbon aerosols at very low concentrations, *J. Phys. Chem., 100*, 15,487-15,493, 1996.

Karcher, B., T. Peter, U.M. Biermann, and U. Schumann, The initial composition of jet condensation trails, *J. Atmos. Sci., 53*, 3066-3083, 1996.

Kotzick, R., U. Panne, and R. Niessne, Changes in condensation properties of ultrafine carbon particles subjected to oxidation by ozone, *J. Aerosol Sci., 28*, 725-735, 1997.

Lammel, G., and T. Novakov, Water nucleation properties of carbon-black and diesel soot particles, *Atmos. Environ., 29*, 813-823, 1995.

Lary, D.J., A.M. Lee, R. Toumi, M.J. Newchurch, M. Pirre, and J.B. Renard, Carbon aerosols and atmospheric photochemistry, *J. Geophys. Res., 102*, 3671-3682, 1997.

Lary, D.J., D.E. Shallcross, and R. Toumi, Carbonaceous aerosols and their potential role in atmospheric chemistry, *J. Geophys. Res., 104*, 15,929-15,940, 1999.

Mandelbrot, B.B., *The Fractal Geometry of Nature*, W.H. Freeman, New York, 1982.

Meakin, P., Fractal aggregates in geophysics, *Rev. Geophys., 29*, 317-354, 1991.

Meakin, P., B. Donn, and G.W. Mulholland, Collisions between point masses and fractal aggregates, *Langmuir, 5*, 510-518, 1989.

Minnis, P., D.F. Young, D.P. Garber, L. Nguyen, W.L. Smith Jr., and R. Palikonda, Transformation of contrails into cirrus during SUCCESS, *Geophys. Res. Lett., 25*, 1157-1160, 1998.

Oh, C., and C.M. Sorensen, The effect of overlap between monomers on the determination of fractal cluster morphology, *J. Colloid Interface Sci., 193*, 17-25, 1997.

Penner, J.E., H. Eddleman, and T. Novakov, Towards the development of a global inventory for black carbon emissions, *Atmos. Env., 27*, 1277-1295, 1993.

Pueschel, R.F., Stratospheric aerosols: Formation, properties, effects, *J. Aerosol Sci., 27*, 383-402, 1996.

Pueschel, R.F., D.F. Blake, K.G. Snetsinger, A.D.A. Hansen, S. Verma, and K. Kato, Black carbon (soot) aerosol in the lower stratosphere and upper troposphere, *Geophys. Res. Lett., 19*, 1659-1662, 1992.

Pueschel, R.F., S. Verma, G.V. Ferry, S.D. Howard, S. Vay, S.A. Kinne, J. Goodman, and A.W. Strawa, Sulfuric acid and soot particle formation in aircraft exhaust, *Geophys. Res. Lett., 25*, 1685-1688, 1998.

Reid, J.S., and P.V. Hobbs, Physical and optical properties of young smoke from individual biomass fires in Brazil, *J. Geophys. Res., 103*, 32,013-32,030, 1998.

Reid, J.S., P.V. Hobbs, R.J. Ferek, D.R. Blake, J.V. Martins, M.R.Dunlap, and C. Liousse, Physical, chemical, and optical properties of regional hazes dominated by smoke in Brazil, *J. Geophys. Res., 103*, 32,059-32,080, 1998.

Rogaski, C.A., D.M. Golden, and L.R. Williams, Reactive uptake and hydration experiments on amorphous carbon treated with $NO_2$, $SO_2$, $O_3$, $HNO_3$, and $H_2SO_4$, *Geophys. Res. Lett., 24*, 381-384, 1997.

Schmidt-Ott, A., New approaches to in situ characterisation of ultrafine agglomerates, *J. Aerosol Sci., 19*, 553-563, 1988.

Schmidt-Ott, A., U. Baltensperger, H.W. Gaggeler, and D.T. Jost, Scaling behavior of physical parameters describing agglomerates *J. Aerosol Sci., 21*, 711-717, 1990.

Schult, I., J. Feichter, and W.F. Cooke, Effect of black car-

bon and sulfate aerosols on the Global Radiation Budget, *J. Geophys. Res., 102*, 30,107-30,117, 1997.

Seinfeld, J.H., and S.N. Pandis, *Atmospheric Chemistry and Physics*, John Wiley, New York, 1998.

Smith, D.M., and A.R. Chughtai, Reaction kinetics of ozone at low concentrations with *n*-hexane soot, *J. Geophys. Res., 101*, 19,607-19,620, 1996.

Smyth, S.B., et al., Factors influencing the upper free tropospheric distribution of reactive nitrogen over the South Atlantic during the TRACE A experiment, *J. Geophys. Res., 101*, 24,165-24,186, 1996.

Sorensen, C.M., and G.D. Feke, The morphology of macroscopic soot, *Aerosol Sci. Technol., 25*, 328-337, 1996.

Sorensen, C.M., and G. Roberts, The prefactor of fractal aggregates, *J. Colloid Interface Sci., 186*, 447-452, 1997.

Strom, J., and S. Ohlsson, In situ measurements of enhanced crystal number densities in cirrus clouds caused by aircraft exhaust, *J. Geophys. Res., 103*, 11,355-11,361, 1998.

Sutherland, D.N., Chain formulation of fine particle aggregates, *Nature, 226*, 1241-1242, 1970.

Tabor, K., L. Gutzwiller, and M.J. Rossi, The heterogeneous interaction of $NO_2$ with amorphous carbon at ambient temperatures, *J. Phys. Chem., 98*, 6172-6186, 1994.

Thouy, R., and R. Jullien, A cluster-cluster aggregation model with tunable fractal dimension, *J. Phys. A Math Gen., 27*, 2953-2963, 1994.

Thovert, J.-F., F. Wary, and P.M. Adler, Thermal conductivity of random media and regular fractals, *J. Appl. Phys., 68*, 3872-3883, 1990.

Turco, R.P., O.B. Toon, and P. Hamill, Heterogeneous physicochemistry of the polar ozone hole, *J. Geophys. Res., 94*, 16,493-16,510, 1989.

Vartiainen, M., S.R. McDow, and R.M. Kamens, Water uptake by sunlight and ozone exposed diesel exhaust particles, *Chemosphere, 32*, 1319-1325, 1996.

Weingartner, E., H. Burtscher, and U. Baltensperger, Hygroscopic properties of carbon and diesel soot particles, *Atmos. Environ., 31*, 2311-2327, 1997.

Witten, T.A., Jr., and L.M. Sander, Diffusion limited aggregation, a kinetic critical phenomenon, *Phys. Rev. Lett., 47*, 1400-1403, 1981.

---

P.M. Adler and D. Coelho, Institut de Physique du Globe de Paris, Tour 24, 4 Place Jussieu, F-75252 Paris, France. (e-mail: adler@n32.rhea.cnusc.fr)

S. Bekki (corresponding author), Service d'Aéronomie du Centre National de la Recherche Scientifique, Université P. et M. Curie, Paris, Boite 102, Couloir 15-14, $5^{eme}$ etage, 4 place Jussieu, 75230 Paris Cedex 05, France. (e-mail: slimane@aero.jussieu.fr)

J.-F. Thovert, Laboratoire des Phénomènes de Transport dans les Mélanges (LPTM), SP2MI, BP 179, 86960-Futuroscope Cedex, France. (e-mail: jft@io.cnusc.fr)

(Received April 7, 1999; revised July 27, 1999;
accepted August 5, 1999.)